Cell, Vol. 93, 111–123, April 3, 1998, Copyright ©1998 by Cell Press

Crystal Structure of the Hemochromatosis Protein HFE and Characterization of Its Interaction with Transferrin Receptor

José A. Lebrón,*‖ Melanie J. Bennett,*‖
Daniel E. Vaughn,*# Arthur J. Chirino,*†
Peter M. Snow,†‡ Gabriel A. Mintier,§
John N. Feder,§ and Pamela J. Bjorkman*†
*Division of Biology
†Howard Hughes Medical Institute
‡Caltech Protein Expression Center
California Institute of Technology
Pasadena, California 91125
§Progenitor Inc.
Menlo Park, California 94025

Summary

HFE is an MHC-related protein that is mutated in the iron-overload disease hereditary hemochromatosis. HFE binds to transferrin receptor (TfR) and reduces its affinity for iron-loaded transferrin, implicating HFE in iron metabolism. The 2.6 Å crystal structure of HFE reveals the locations of hemochromatosis mutations and a patch of histidines that could be involved in pH-dependent interactions. We also demonstrate that soluble TfR and HFE bind tightly at the basic pH of the cell surface, but not at the acidic pH of intracellular vesicles. TfR:HFE stoichiometry (2:1) differs from TfR: transferrin stoichiometry (2:2), implying a different mode of binding for HFE and transferrin to TfR, consistent with our demonstration that HFE, transferrin, and TfR form a ternary complex.

Introduction

Hereditary hemochromatosis (HH) is a disease characterized by the excessive deposition of iron in different organs of the body leading to multiorgan dysfunction. HH is the most common autosomal recessive disorder affecting individuals of Northern European descent. Approximately 1 in 200 to 1 in 400 Caucasian individuals have HH, leading to an estimated carrier frequency of between 1 in 8 and 1 in 10 (Merryweather-Clarke et al., 1997, and references therein). A candidate gene for HH was identified near, but not in, the major histocompatibility complex (MHC) (Feder et al., 1996). The gene product HFE is a 343 residue type I transmembrane glycoprotein that is homologous to class I MHC proteins and associates with the class I light chain β2-microglobulin (β2m) (Feder et al., 1996). Between 69% and 100% of HH patients are homozygous for a mutation (845G→A) that converts Cys-260 to a tyrosine (reviewed in Cuthbert, 1997), preventing formation of a disulfide bond in the α3 domain and abrogating β2m association as well as cell-surface expression of the protein (Feder et al., 1997; Waheed et al., 1997). A second mutation that converts His-41 to aspartate increases the relative risk of developing hemochromatosis in individuals who are heterozygous for the Cys260Tyr mutation (Feder et al., 1996; Beutler, 1997). Unlike the Cys260Tyr substitution, the His41Asp substitution does not prevent β2m association or cell surface expression (Feder et al., 1997; Waheed et al., 1997). (Our numbering system begins with residue 1 of the mature protein and differs from previous systems that began numbering at the intitial methionine [see Experimental Procedures]. Thus, the residues we refer to as Cys-260 and His-41 correspond to Cys-282 and His-63 in earlier publications.)

The homology between HFE and MHC molecules does not suggest an obvious role for HFE in iron homeostasis, since class I MHC molecules function in peptide presentation to T cells. A connection between HFE and iron absorption was recently made with the demonstration that HFE associates with transferrin receptor (TfR) (Parkkila et al., 1997; Feder et al., 1998) and decreases its affinity for iron-bound transferrin (diferric Tf [Fe-Tf]) by 5- to 10-fold (Feder et al., 1998). The Tf/TfR system is a well-established pathway by which cells absorb iron. Fe-Tf in the blood binds to cell-surface TfR and triggers endocytosis of the Tf/TfR complex (reviewed in Richardson and Ponka, 1997). Upon exposure to the acidic pH of the endosome, iron is released from Tf and enters a chelatable intracellular pool from which it is utilized for the metabolic needs of the cell or incorporated into the storage protein ferritin. Apo-Tf remains bound to TfR at the low pH of the acidic vesicle (≤pH 6.0) and the apo-Tf/TfR complex is then recycled to the cell surface where apo-Tf dissociates at the pH of blood (∼pH 7.4). The role of TfR in iron uptake has been well characterized but the association with HFE was previously unnoticed, perhaps because HFE is not expressed in commonly used cultured cell systems (e.g., HeLa cells, 293 cells; J. N. F, unpublished data), possibly an adaptive response to allow increased iron uptake.

The functional consequences of the primary mutation in HFE, Cys260Tyr, were addressed by the demonstration that, unlike wild-type HFE, the Cys260Tyr mutant does not interact with TfR and therefore does not decrease TfR's affinity for Fe-Tf (Feder et al., 1998). In contrast, the His41Asp mutant form of HFE still interacts with TfR but does not decrease the affinity for Fe-Tf to the same extent as wild-type HFE. The results described above suggest that when HFE is expressed in the same cell as TfR, less Tf-associated iron will be taken into the cell. In the absence of HFE, as in the hemochromatotic individual carrying the Cys260Tyr mutation, more iron would be brought into cells, ultimately resulting in increased iron deposition in cells that normally use HFE for modulation of iron intake.

In this study, we have determined the X-ray crystal structure of a soluble form of human HFE and characterized the interactions between HFE, Tf, and TfR. Combined with the observation that HFE reduces the affinity of TfR for Fe-Tf (Feder et al., 1998), our results support a model in which HFE is involved in the canonical iron absorption pathway and regulates iron intake by a

‖These authors contributed equally to this work.
#Present address: Cold Spring Harbor Laboratory, 1 Bungtown Road, Cold Spring Harbor, NY 11724.

Table 1. Data Collection and Refinement Statistics for HFE

Unit cell dimensions	
a, b, c (Å)	68.8, 100.1, 147.6
Space group	$P2_12_12_1$
Temperature (°C)	−150
Data Processing	
Resolution (Å)	15.0–2.6 (2.7–2.6)
Observations	187,780
Unique reflections	32,145 (3,435)
Completeness (%)	98.1 (96.7)
I/σ	23.7 (3.2)
R_{merge}[a] (%)	5.9 (42.1)
Refinement	
Resolution	15.0–2.6
Reflections in working set	30,215
Reflections in test set	1,555
R_{free}[b] (%)	27.7
R_{cryst}[b] (%)	23.3
Rms deviations from ideality	
Bond lengths (Å)	0.009
Bond angles (deg)	1.4
Number of nonhydrogen atoms	
Protein	6068
Water	25

[a] R_{merge} (I) = $(\Sigma|(I(i) - <I(h)>|)/\Sigma I(i)$, summed over all reflections and all observations, where I(i) is the ith observation of the intensity of the hkl reflection and $<I(h)>$ is the mean intensity of the hkl reflection.

[b] R_{cryst} (F) = $\frac{\Sigma_h||F_{obs}(h)|-|Fc(h)||}{\Sigma_h|F_{obs}(h)|}$, where F_{obs} and F_c are the observed and calculated structure factor amplitudes for the hkl reflection. R_{free} is calculated for a set of reflections that were not included in atomic refinement (Brünger, 1992b).

mechanism that involves binding to TfR in a pH-dependent manner.

Results

Structure of HFE

Soluble HFE/β2m heterodimers were expressed in Chinese hamster ovary (CHO) cells. The crystal structure was determined to 2.6 Å by molecular replacement using a 2.0 Å structure of the human class I MHC molecule HLA-A2 (Collins et al., 1994). The refined structure has good stereochemistry (Table 1) and 94% of the residues within allowed regions of the Ramachandran plot as defined by Kleywegt and Jones (1996).

The overall structure of HFE resembles MHC class I molecules (such as HLA-A2, with which it shares 37% sequence identity). In both, the α1 and α2 domains form a platform composed of eight antiparallel β strands topped by two antiparallel α helices (Figure 1B) positioned on top of two immunoglobulin constant-like domains: α3 and the light chain β2m (Figure 1A). The individual domains in HFE can be superimposed upon the corresponding domains in HLA-A2 with rms deviations of less than 1.5 Å for most Cα atoms, comparable to superpositions of two other class I MHC-related proteins: the neonatal Fc receptor (FcRn) (Burmeister et al., 1994a) and CD1, a class Ib MHC protein (Zeng et al., 1997) (see Experimental Procedures). In HFE, as in class I and class I-related proteins, α3 and β2m interact with a symmetry that deviates from the pseudo-dyad symmetry relating antibody constant domains. Specifically, the HFE domains are related by a 161° rotation and a 13 Å translation. This relative orientation is in the range seen for the α3-β2m relationship in class I molecules (146°-160° rotation, 13–14 Å translation), CD1 (170° rotation, 12 Å translation) (reviewed in Zeng et al., 1997), and FcRn (157° rotation, 13 Å translation) (Burmeister et al., 1994a).

The HFE residue involved in the Cys260Tyr mutation is in the α3 domain, where it disulfide bonds with Cys-203 (Figures 1A and 1C). His-41, the residue substituted in the His41Asp mutation, is in a loop in the α1 domain, where it forms a salt bridge with Asp-73 (Figure 1B). Substitution of an aspartate at position 41 would be unlikely to affect the overall protein fold but would disrupt the salt bridge with Asp-73, perhaps leading to a local rearrangement of the loop to avoid juxtaposition of two negative charges.

The surface of HFE includes a cluster of four histidine residues accounting for one-third of the total histidines in the human HFE heavy chain (Feder et al., 1996) (Figure 1D). The clustering of these histidines with a nearby tyrosine (HFE Tyr-118) bears some resemblance to the composition of mononuclear iron–binding sites in several proteins (Howard and Rees, 1991). Thus far, analyses of crystals soaked at near-neutral or basic pH in iron (10 mM Fe(III)-NTA or 10 mM $Fe(II)(NH_4)_2SO_4$) or chemically similar metals (10 mM $NiCl_2$ or 10 mM $MnCl_2$) have not yielded evidence of metal binding in this region (M. J. B., J. A. L., and P.J.B., unpublished data). However, the conditions under which the crystals were soaked may not have been optimal for metal binding.

Groove Narrowing in HFE Prevents Peptide Binding

Although the overall structure of HFE resembles class I MHC molecules, HFE lacks a functional peptide-binding groove. Whereas class I molecules bind short (8–10 residues) peptides (Rammensee et al., 1993), peptides are not associated with HFE (Table 2). The crystal structure reveals the reason for HFE's lack of peptide binding: its counterpart of the MHC peptide-binding groove is narrowed by a translation of the α1 helix bringing it ~4 Å closer to the α2 helix (Figure 2A). A striking feature of the HFE groove is that the entire α2 helix is almost identically positioned to the α2 helix in class I molecules, whereas in the MHC-related molecules FcRn and CD1 both helices are repositioned.

The narrower groove in HFE results in burial of residues analogous to those forming pockets that interact with peptides in class I binding clefts. Class I pockets A and F accommodate the N and C termini of bound peptides and are lined with mostly conserved residues, while the intermediate pockets (B to E) interact with peptide side chains and contain residues that vary (Figure 2B; Saper et al., 1991; Matsumura et al., 1992). Overall, about half of the HFE residues located in positions analogous to class I pockets A through F are buried, preventing them from an interaction with peptide (Table 3). In class I pocket A, tyrosines 7, 59, 159, and 171 interact with the peptide N terminus, and Trp-167 is at the groove rim in many class I alleles (Figure 2B). In HFE, only two of the tyrosines are conserved (HFE Tyr-10 and Tyr-160) and Tyr-10 is buried (Table 3). In addition, the side chain of HFE Gln-168 (class I residue 167)

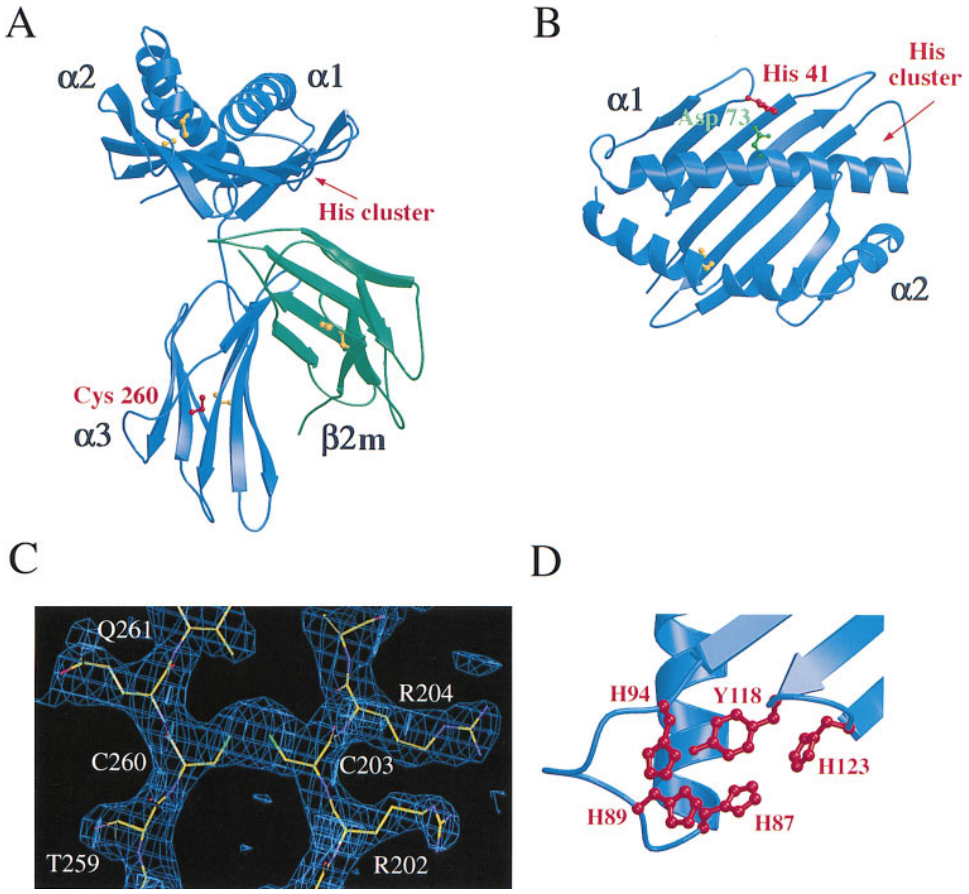

Figure 1. Crystal Structure of HFE and Comparison to a Class I MHC Molecule

(A) Ribbon diagram shows that HFE resembles class I molecules in the fold of the heavy chain (blue) and in its association with the β2m light chain (green). Cys-260, the residue substituted in the Cys260Tyr mutation, disulfide bonds with Cys-203.

(B) Ribbon drawing of a top view of the HFE α1-α2 platform. His-41 (red), the site of the His41Asp mutation, interacts with Asp-73 (green).

(C) The HFE model in the region of the Cys-260—Cys-203 disulfide bond is shown superimposed on a $2F_o-F_c$ annealed omit electron density map (Hodel et al., 1992) contoured at 1σ. The average B factor for the residues shown is 48 Å^2.

(D) Close-up of a histidine cluster and nearby tyrosine located underneath the right-hand side of the platform. His-94 is found in class I MHC molecules (class I His-93); His-89 and His-123 are present only in human (Feder et al., 1996), rat (EMBL accession number AJ001517), and mouse (Hashimoto et al., 1997) HFE. His-87 is present in human, but not mouse or rat, HFE.

(A), (B), and (D) were made with Molscript (Kraulis, 1991) and rendered with Raster3D (Merritt and Murphy, 1994). (C) was prepared with O (Jones and Kjeldgaard, 1997).

points into the groove to occlude pocket A (Figure 2C) in a manner reminiscent of Arg-164 in FcRn (Burmeister et al., 1994a).

In addition to resulting in burial of pocket residues, the groove narrowing causes several residues in HFE to occupy positions that would clash with a bound peptide. To identify only those HFE residues that would clash with all bound peptides regardless of sequence, the side chains in four defined nonameric peptides bound to HLA-A2 (Madden et al., 1993) were truncated to alanines and superimposed upon HFE. In total, eight side chains from the HFE α1 helix and two side chains from the α2 helix are incompatible with peptide binding (Figure 2C). The clashes are caused both by the translation of the α1 helix toward the α2 helix and by the presence of larger side chains in HFE as compared to class I (HFE Leu-69 versus class I Val-67, HFE Trp-72 versus class I His-70, HFE Met-75 versus class I Thr-73, and HFE Arg-153 versus class I Val-152). Additional HFE residues probably also contribute to HFE's inability to bind peptides with side chains larger than alanine; e.g., Trp-114 on the HFE groove floor (Figure 2C).

The HFE counterpart of the peptide-binding groove is distinct from the grooves in two other MHC class I–related proteins of known structure (Figure 2A): FcRn, which has an almost completely closed groove (Burmeister et al., 1994a), and CD1 (Zeng et al., 1997), which contains a deep hydrophobic groove that binds lipids (Beckman et al., 1994) and long (12–22 residues) hydrophobic peptides (Castaño et al., 1995). The total surface area of the groove in HFE (~415 Å^2) is intermediate between that in FcRn (~235 Å^2) and class I molecules (~760 Å^2). CD1 has a narrower but deeper groove than class I grooves, with the most extensive surface area of all (~1440 Å^2) (see Experimental Procedures).

The structural rearrangements resulting in grooves of various sizes and shapes differ in HFE, FcRn, and CD1. In contrast to HFE, in which the α2 helix is positioned similarly to its counterpart in class I molecules, the α2 helix of FcRn or CD1 is kinked about a hinge point near

Table 2. Amino Acids Recovered from Acid Elutions[a]

Cycle Number	HFE	FcRn	UL18
1	2.1	5.9	86.0
2	0.5	4.7	75.1
3	0.4	0.7	36.9
4	0.8	7.6	19.8
5	0.0	0.0	11.3
6	3.5	0.0	4.0
7	1.0	0.2	3.7
8	0.0	0.6	6.5
9	1.9	9.5	4.3
10	0.0	0.3	1.3

[a] Total yield (pmols) of amino acids from each N-terminal sequencing cycle for acid eluates derived from equivalent amounts of HFE, FcRn, and UL18. Previous studies established that UL18 and classical class I molecules, but not FcRn, associate with endogenous peptides when expressed as soluble proteins in CHO cells (Chapman and Bjorkman, 1998, and references therein). Only those amino acid residues that showed an increase in the absolute amount recovered compared to the previous cycle were considered significant. Analysis of the HFE and FcRn eluates by matrix-assisted, laser desorption, time-of-flight mass spectrometry using a PerSeptive Biosystems ELITE mass spectrometer did not reveal the presence of N-terminally blocked peptides (data not shown).

a proline. HFE is the only class I homolog that has a proline at this position (HFE Pro-166, FcRn Pro-162, and CD1 Pro-169) in which a kink is not seen. Instead, HFE Pro-166 is accommodated without significant structural rearrangements relative to class I molecules (Figure 2A), which contain a valine at this position (Val-165). The reason appears to be that a local distortion, perhaps related to a neighboring disulfide bridge involving class I Cys-164, occurs at this point in class I molecules, and the -NH group of the subsequent class I residue (Val-165) is not hydrogen bonded in the helix. Thus, this position in the α2 helix can accommodate a proline as occurs in HFE without altering the structure.

HFE Binds Tightly to TfR at pH 7.5 but Not at pH 6

In order to further characterize the interaction of HFE with TfR, we expressed a soluble form of TfR (residues 121–760) corresponding to a previously characterized proteolytic fragment purified from human placenta (Turkewitz et al., 1988a). Since TfR is normally a disulfide-linked homodimeric type II membrane glycoprotein (Schneider et al., 1984), we first verified that the properties of soluble recombinant TfR are similar to those of its membrane-bound counterpart. Analytical ultracentrifugation demonstrated that soluble TfR is dimeric (data not shown). In a surface plasmon resonance (SPR) based assay, soluble TfR binds Fe-Tf with a K_D ~3 nM at pH 7.5 (Figure 3; Table 4; K_D's cited in the text are the median of the range of values derived under different experimental conditions), consistent with the affinity of Fe-Tf for membrane-bound TfR (5 nM; Richardson and Ponka, 1997, and references therein). Soluble TfR also retains membrane-bound TfR's pH-dependent affinity for apo-Tf, binding at pH 6.0 (K_D ~8 nM) but not at pH 7.5 (Figure 3; Table 4). Since soluble TfR retains the binding properties and physical characteristics of membrane-bound TfR and because previous studies implied that the HFE-TfR interaction does not require the transmembrane domain of either protein (Feder et al., 1998), soluble TfR is an appropriate reagent for analyses of HFE-TfR binding.

In order to measure the affinity between HFE and TfR, HFE was covalently immobilized to a biosensor chip using primary amine chemistry (see Experimental Procedures). At pH 7.5, TfR binds immobilized HFE with high affinity (K_D ~0.6 nM). The interaction was not affected by the addition of the iron chelator pyrophosphate (PP_i) during the assay (data not shown), demonstrating that HFE binding to TfR does not require iron. In contrast to the high affinity binding between TfR and HFE, Tf does not bind HFE (Table 4). Thus, the HFE-mediated decrease in the affinity of TfR for Fe-Tf (Feder et al., 1998) does not involve a direct interaction between HFE and Tf.

When the HFE-TfR interaction was monitored at pH 7.5 in the reverse orientation by injecting HFE over primary amine–coupled TfR, the affinity is significantly lower (K_D ~240 nM) (Table 4). In order to investigate whether this decreased affinity was a result of the method of TfR immobilization (see Experimental Procedures), we injected HFE over TfR that was noncovalently coupled via its 6xHis-tag to a biosensor chip derivatized with nickel nitrilotriacetic acid (Ni-NTA). However, since HFE interacts directly with the Ni-NTA chip at high HFE concentrations (>50 nM; Figure 3C) (perhaps due to nickel binding to the His cluster on HFE; Figure 1D), we could not obtain a precise value for the K_D of this interaction. Nonetheless, the approximate affinity and dissociation rate derived from the interaction of HFE with His-tagged TfR captured on the Ni-NTA chip are consistent with those derived using covalently immobilized TfR and not with those derived using soluble TfR and immobilized HFE (Figure 3; Table 4). Thus, TfR binds to immobilized HFE more tightly than HFE binds to immobilized TfR.

The biosensor studies demonstrate that TfR and HFE interact strongly with an affinity either comparable to the affinity of TfR for its Tf ligand or no more than 100-fold weaker (Figure 3; Table 4). We cannot ascertain the reason for the coupling-dependent affinity difference of the HFE-TfR interaction, but note that coupling-dependent differences have been observed in other biosensor assays (Kuziemko et al., 1996; Vaughn and Bjorkman, 1997). In those cases, the higher affinity values corresponded more closely to values derived from cell binding assays. By analogy, we expect the higher affinity (K_D ~0.6 nM; Table 4) to be more relevant for the physiological interaction of TfR and HFE so that TfR binds HFE at least as tightly as it binds its Tf ligand. In vivo, complex formation between TfR and HFE is likely to be even more favored than predicted from the affinities determined in these biosensor studies due to tethering of the two proteins on the same membrane.

At pH 6.0, HFE shows either only very weak binding (K_D > 10 mM) or no detectable binding to TfR (Table 4; Figures 3A and 3B). Thus, the TfR-HFE binding affinity drops from nanomolar to essentially undetectable over a change in pH of less than two units (Table 4). Histidine residues, with their near-neutral pK_a's, are likely candidates to mediate pH-dependent binding over this pH

range (Fersht, 1985). Specifically, neutral histidines could be involved in binding of TfR and HFE at the pH of the cell surface (∼pH 7.4) with protonation of histidines in acidic vesicles (∼pH 6.0) then mediating the dissociation of TfR and HFE. The prominent patch of histidines in HFE (Figure 1D) and/or His-41, the site of one of the HH mutations, could be involved in these sorts of pH-dependent interactions (see Discussion).

HFE and Tf Bind to TfR with Different Stoichiometries and Can Bind Simultaneously to Form a Ternary Complex

We used a gel filtration assay to determine the stoichiometry of the interaction of TfR with Tf and with HFE. At pH 7.5, TfR and Fe-Tf form a complex with 2:2 stoichiometry (Figure 4), consistent with earlier results (Enns and Sussman, 1981) and with the hypothesis that each polypeptide chain in the TfR homodimer binds to one Tf molecule. At the same pH, TfR complexes with HFE with 2:1 stoichiometry (Figure 4), corresponding to one TfR homodimer binding only one HFE. At pH 6.0, HFE and TfR do not form a complex that is observed on the sizing column (data not shown), as expected from the biosensor studies (Table 4).

The observation that HFE and Tf bind to TfR with different stoichiometries implies that TfR uses a different mode of binding to interact with each protein, which in turn suggested that a ternary complex of TfR, Tf, and HFE could form. We used an anti-HFE monoclonal antibody (1C3) that does not interfere with HFE binding to TfR to investigate whether Tf coimmunoprecipitates along with HFE and TfR. HFE, TfR, and Fe-Tf were incubated at a 1:2:2 molar ratio (corresponding to one HFE, one TfR homodimer, and two molecules of Fe-Tf), followed by immunoprecipitation. SDS-PAGE analysis demonstrates that bands corresponding to HFE, TfR, and Fe-Tf are present regardless of the order of addition of the proteins (Figure 5).

Discussion

HFE was initially implicated in iron metabolism by the discovery that it is mutated in patients afflicted with HH, an iron-overload disorder (Feder et al., 1996). The majority of HH patients are homozygous for a single site mutation leading to the Cys260Tyr substitution (reviewed in Cuthbert, 1997) that disrupts the interaction between HFE and its β2m light chain and prevents cell-surface expression (Feder et al., 1997; Waheed et al., 1997). The 2.6 Å crystal structure of HFE confirms that, as predicted from its sequence (Feder et al., 1996), HFE closely resembles class I MHC molecules and that Cys-260 is involved in a disulfide bridge analogous to those found in class I MHC α3 domains. The residue involved in a second mutation found in some HH patients (His41Asp) is located in a loop within the α1 domain. This mutation may alter the structure of the protein locally by a loop rearrangement to avoid juxtaposition of the substituted aspartate with Asp-73, a residue with which His-41 normally interacts. The existence of these mutations in HH patients implies that properly folded HFE is required for prevention of iron overload.

Insight into the molecular mechanism of HFE in iron uptake regulation is provided by the recent discovery that HFE binds to TfR (Parkkila et al., 1997; Feder et al., 1998) and thereby reduces its affinity for Fe-Tf (Feder et al., 1998). The HH mutations either eliminate the binding of HFE to TfR (Cys260Tyr) or alter HFE's ability to reduce the affinity between TfR and Fe-Tf (His41Asp) (Feder et al., 1998). How perturbation of the HFE-TfR association might result in increased iron absorption in the small intestine, as seen in patients with HH (McLaren et al., 1991), will require additional studies (for further discussion see Feder et al., 1998). However, a higher affinity between TfR and Fe-Tf due to the absence of fully functional HFE could lead to increased iron uptake by cells in some tissues, ultimately causing excess iron deposition in the major organs, a primary defect in HH (Bacon and Tavill, 1996).

To further define the HFE-TfR association, we have begun to characterize the interaction between soluble forms of HFE and TfR. Considering that HFE was only recently identified as a component in the TfR pathway, HFE and TfR form a surprisingly high affinity complex at the slightly basic pH found at the cell surface (K_D ∼0.6 nM), while at the acidic pH corresponding to intracellular vesicles there is little or no binding of HFE to TfR. The pH-dependent affinity of the HFE-TfR interaction is reminiscent of the interaction between TfR and apo-Tf and of the interaction between FcRn and its immunoglobulin G (IgG) ligand, interactions that each show a sharp pH dependence in the range between pH 6 and pH 7.5 (reviewed in Richardson and Ponka, 1997; Junghans, 1997). In the TfR-apo-Tf and FcRn-IgG systems, the receptors' functions involve trafficking through acidic compartments as a complex with ligand and release of ligand at the slightly basic pH of blood. The sharp pH dependence of the HFE-TfR interaction, an unusual feature of a protein–protein interaction unless it is required for pH-regulated binding during trafficking, implies that HFE enters the cell along with TfR-Tf complexes, then dissociates from TfR in acidic vesicles. Thus, studies of HFE trafficking and/or recycling might be pertinent to HFE's role in the regulation of iron homeostasis.

Histidine residues are likely candidates for mediating pH-dependent protein interactions at pH values near neutral. Histidines have a pK_a of 6.6 in model compounds (Fersht, 1985) and are therefore likely to be neutral at the basic pH of blood and to carry a positive charge at the pH of acidic intracellular vesicles. The FcRn-IgG system is a well-characterized example of a pH-dependent affinity difference mediated through titration of histidines (Vaughn and Bjorkman, 1998). By analogy, the pH dependence of the HFE-TfR interaction could be due to a favorable interaction at neutral or slightly basic pH involving uncharged histidines on one or both proteins, which becomes unfavorable upon acquiring positive charge(s) by protonation at acidic pH. The distribution of histidines in TfR is unknown, but the HFE structure includes an intriguing patch of histidines (Figure 1D) that could act as a pH-dependent switch to modulate the interaction. In addition to the potential involvement of the clustered histidines in intermolecular pH-dependent interactions, HFE His-41 is involved in an intramolecular pH-dependent interaction in that it forms a salt bridge

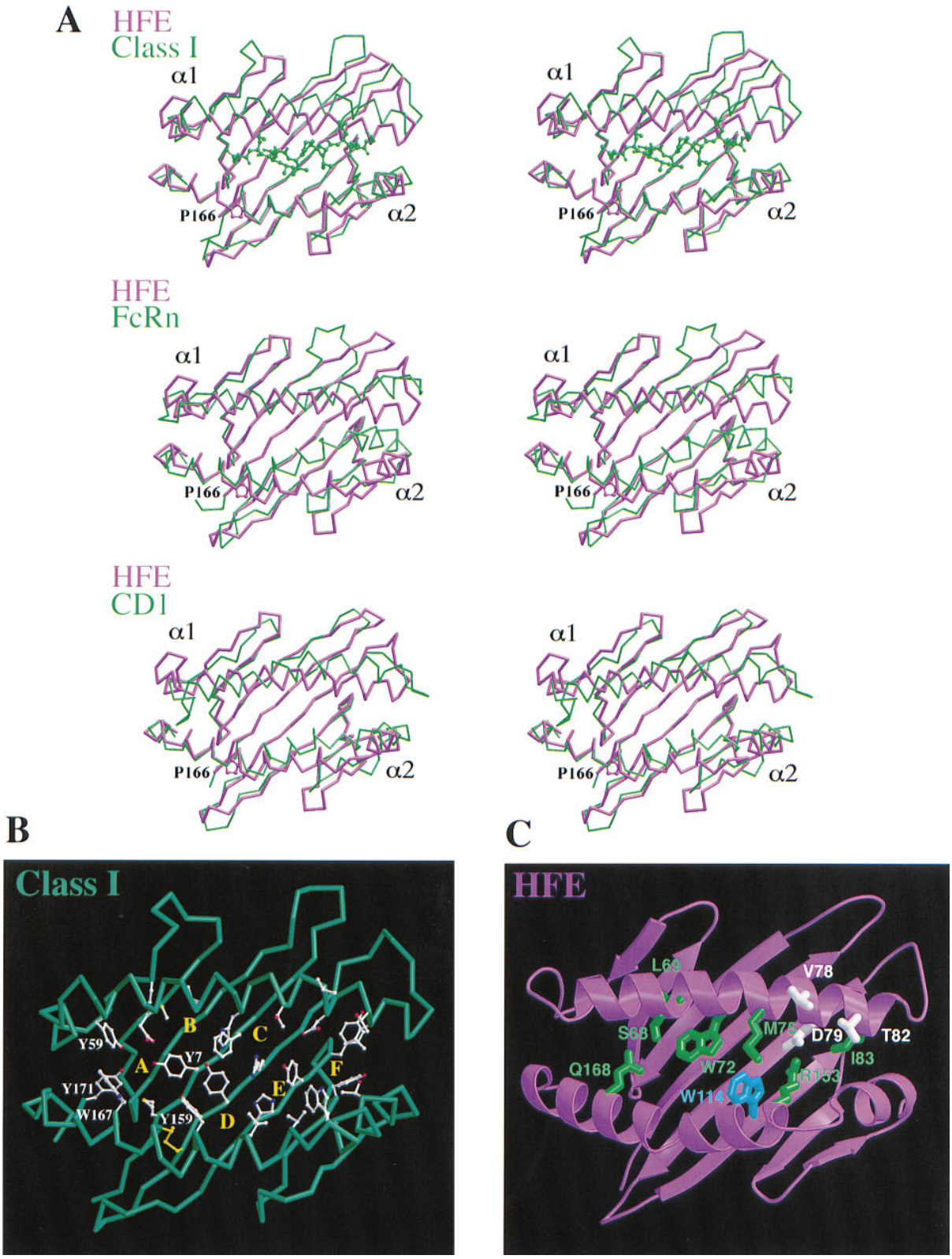

Figure 2. The Counterpart of the Class I Peptide-Binding Groove is Narrowed in HFE by Translation of the α1 Helix

(A) Cα stereo superpositions based on Cα atoms in the platform β strands of HFE with class I and class I–related proteins. Top, HLA-A2 (green, including a ball-and-stick representation of bound peptide; PDB code 2CLR) and HFE (magenta). Heavy chains share 37% amino acid sequence identity. Middle, Rat FcRn (green; PDB code 1FRU) and HFE (magenta). Heavy chains share 28% sequence identity. HFE Pro-166 (labeled) is analogous to FcRn Pro-162, located at a kink in the FcRn α2 helix. Bottom, Mouse CD1 (green) (Zeng et al., 1997) and HFE

Table 3. Comparison of Residues in Peptide-Binding Grooves of HLA-A2 and HFE

HLA-A2	Pocket[a]	HFE	Pocket[a]	Clash with Peptide?[b]
Met-5	A	Leu-8	Buried	No
Tyr-7	A, B	Tyr-10	Buried	No
Phe-9	B, C	Phe-12	Buried	No
Met-45	B	Val-46	B	No
Tyr-59	A	Met-61	A	No
Glu-63	A, B	Leu-65	A, B	No
Lys-66[c]	A	Ser-68	A	Yes
Val-67	B	Leu-69	B	Yes
His-70	B, C	Trp-72	B, C	Yes
Thr-73[c]	C	Met-75	C	Yes
Val-76	Not in a pocket	Val-78	Not in a pocket	Yes
Asp-77[c]	F	Asp-79	Buried	Yes
Thr-80[c]	F	Thr-82	F	Yes
Leu-81	F	Ile-83	Buried	Yes
Arg-97	C, E	Val-98	Buried	No
Tyr-99	A, B, C, D	Leu-100	Buried	No
His-114	C, D, E	Trp-114	C, D, E	No
Tyr-116	C, F	Tyr-116	Buried	No
Tyr-118	F	Tyr-118	F	No
Tyr-123	F	His-123	Buried	No
Ile-124	F	Leu-124	Buried	No
Thr-143	F	Thr-143	Buried	No
Trp-147	E, F	Trp-147	E, F	No
Val-152	E	Arg-153	E	Yes
Leu-156	D, E	Asn-157	D, E	No
Tyr-159	A, D	Tyr-160	A, D	No
Trp-167	A	Gln-168	A	Yes
Tyr-171	A	Leu-172	A	No

[a] Pocket residues in the peptide binding groove of HLA-A2 are defined as having $\geq$5.0 Å^2 of solvent accessible surface area with a 1.4 Å probe radius but $<$5.0 Å^2 with a 5.0 Å probe radius. Analogous residues in HFE are listed for comparison. "Buried" indicates an HFE residue that is inaccessible to a 1.4 Å probe. Surface areas were calculated excluding water molecules and bound peptide using the coordinates of HLA-A2 (PDB code 2CLR) and HFE.

[b] Steric clashes with polyalanine peptides defined as described (Figure 2C).

[c] Residues that have accessible surface in the binding cleft of HLA-A2 and hence constitute pockets (Saper et al., 1991), but are accessible to a 5.0 Å probe and do not meet the criterion for pocket residues described above.[a]

with Asp-73 (Figure 1B) that would be more stable at acidic compared to basic pH. Interestingly, this residue is mutated to aspartate in some HH patients (Feder et al., 1996; Beutler, 1997), destroying its potential to form a pH-dependent salt bridge.

Because HFE is structurally similar to MHC molecules, another candidate for its ligand recognition site is the HFE counterpart of the MHC peptide-binding groove, a characteristic feature of classical class I molecules and CD1. Biochemical and structural analyses demonstrate that HFE does not bind peptides or other small molecules in this region. Although the region of HFE involved in ligand binding remains to be established, the narrowing of the HFE groove compared to class I molecules suggests that HFE does not use what remains of its groove for ligand recognition in a manner analogous to peptide binding in MHC molecules. That is, although TfR could bind to this general area on HFE, the HFE groove is not large enough to accept a loop from TfR in the position where a peptide would bind to a class I molecule. Alternatively, HFE may use an entirely different surface for binding ligands. A precedent for an MHC-related molecule that binds ligands using a molecular surface other than the groove is found in the example of FcRn. Like HFE, FcRn functions in a recognition event (binding and transporting IgG) that bears no resemblance to the antigen presentation functions of classical class I MHC molecules and CD1, and its counterpart of the MHC peptide-binding groove is closed and is not the binding site for IgG (Burmeister et al., 1994b).

The interaction between HFE and TfR will ultimately require a detailed characterization of both proteins, which we have initiated by an analysis of their complex. Our observation that the stoichiometry of TfR's interaction with Fe-Tf (2:2) differs from the stoichiometry of its interaction with HFE (2:1) implies that HFE and Tf bind

(magenta). Heavy chains share 22% sequence identity. HFE Pro-166 (labeled) is analogous to CD1 Pro-162, located at a kink in the CD1 α2 helix.

(B) Peptide-binding groove of HLA-A2 with labeled binding pockets.

(C) HFE counterpart of the class I binding groove showing residues that would clash with a bound peptide. HFE side chains shown in white (same in HFE and HLA-A2) and green (different in HFE and HLA-A2) have at least two steric clashes with polyalanine versions of four different nonameric peptides (from HLA-A2 structures, PDB codes 1HHG, 1HHI, 1HHJ, and 1HHK; Madden et al., 1993) that were superimposed upon HFE after alignment of HLA-A2 and HFE. Steric clashes are defined as occurring when atoms are closer than the sum of their van der Waals radii minus 0.4 Å. The blue side chain would clash with peptides containing side chains larger than alanine.

All panels were made with Molscript (Kraulis, 1991) and rendered with Raster3D (Merritt and Murphy, 1994).

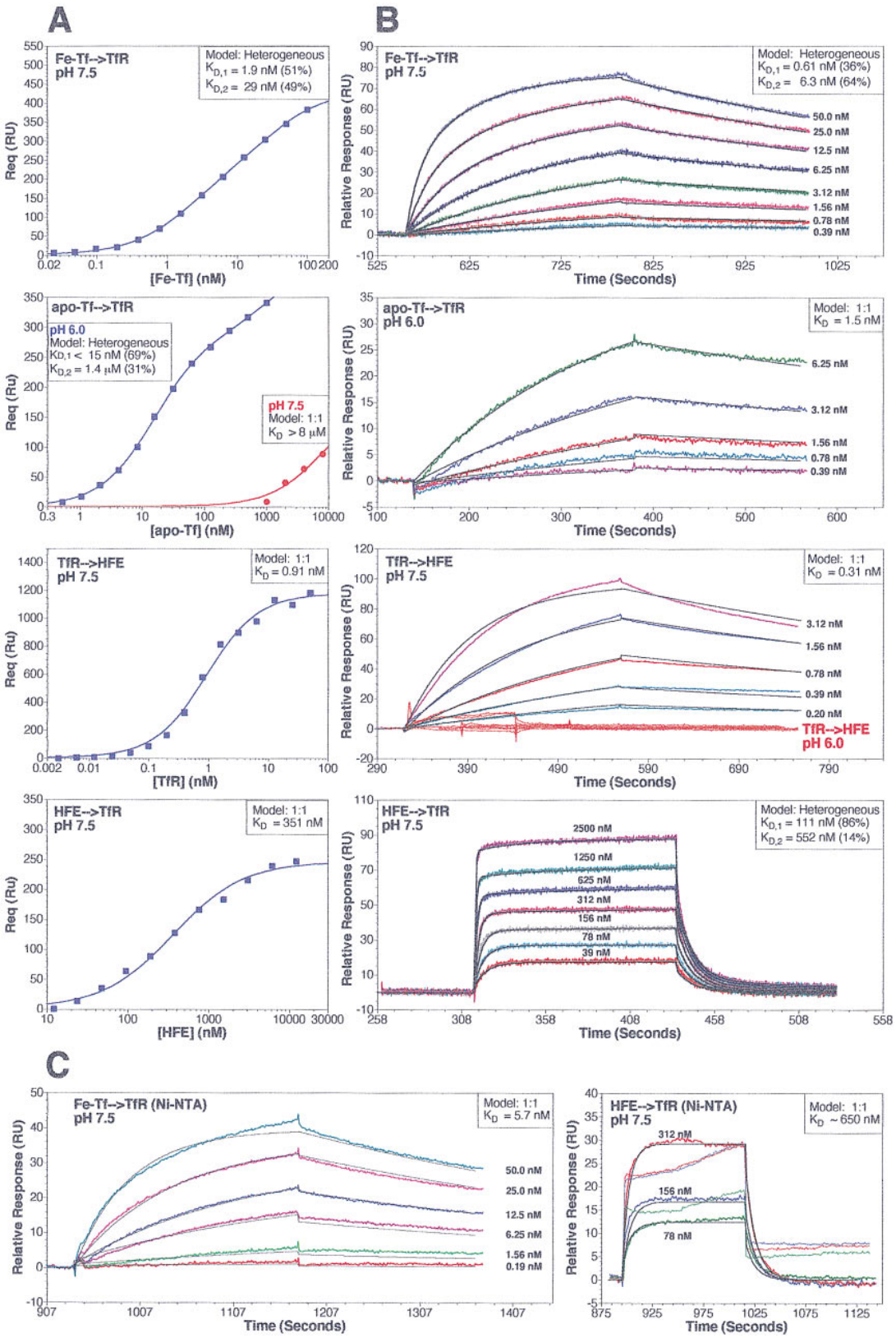

Figure 3. Biosensor Assays of TfR-Tf and TfR-HFE Binding

In each panel, the injected protein is indicated in front of an arrow pointing to the immobilized protein (coupled covalently via primary amines [A and B] or coupled noncovalently via a 6xHis-tag to a Ni-NTA chip [C]). The model used to fit the data is listed along with a derived affinity constant(s). "Heterogeneous" refers to two classes of noninteracting binding sites on the coupled protein with different K_D's ($K_{D,1}$ and $K_{D,2}$),

differently to TfR, most likely to distinct regions of the receptor (Figure 4). Regardless of where these proteins bind to TfR, the finding that HFE and Fe-Tf can bind simultaneously to TfR to form a ternary complex demonstrates that HFE does not occlude both Tf-binding sites on TfR. Since TfR is homodimeric (Schneider et al., 1984; Turkewitz et al., 1988a), it seems reasonable to postulate a 2-fold symmetric structure for a Tf-TfR complex in which each polypeptide chain binds to one Tf to produce 2:2 stoichiometry (Enns and Sussman, 1981). The finding that only one HFE binds to a TfR homodimer raises the possibility that HFE binding induces asymmetry in the TfR homodimer, resulting in only a single optimal HFE-binding site. The resulting asymmetric receptor might then be expected to bind Fe-Tf with lower affinity.

The crystal structure of HFE and the characterization of its interaction with TfR reported here provide a framework for studies to elucidate the role of HFE in iron homeostasis under normal circumstances and in the disease state caused by iron overload. In addition, the structure of HFE provides the first example of the use of the MHC fold for a recognition event outside of the immune system. Despite differences in function and ligand specificity, the three-dimensional structures of classical class I molecules CD1, FcRn, and HFE are remarkably similar, raising the intriguing questions of why and how evolution has selected the MHC fold for such diverse biological roles.

Experimental Procedures

Expression, Purification, and Characterization of Soluble HFE

A construct encoding soluble HFE (residues 1–275 of the mature protein) was subcloned after sequencing into the expression vector PBJ5-GS that carries the glutamine synthetase gene as a selectable marker and means of gene amplification in the presence of methionine sulfoximine (Bebbington and Hentschel, 1987). HFE and human β2m expression vectors were cotransfected into CHO cells. Selection, amplification, and maintenance of methionine sulfoximine–resistant cells and identification of HFE-expressing cells were done as described (Chapman and Bjorkman, 1998). HFE/β2m heterodimers were isolated from supernatants of cells grown in a hollow fiber bioreactor device (Unisyn Fibertec) at yields up to 35 mg/liter using an immunoaffinity column made with an anti-HFE monoclonal antibody (1C3) (J. A. L., H. Shen, P. J. B., and S. Ou, unpublished data). HFE was eluted from the 1C3 column using 50 mM diethylamine (pH 11.0) into tubes containing 1M monobasic sodium phosphate, then further purified by anion exchange chromatography using an FPLC mono Q column (Pharmacia Biotech). N-terminal sequence analysis of purified protein yielded the sequences RLLRSHSLHYLF and IQRTPKIQVYSR corresponding to correctly processed mature HFE and human β2m. In our numbering system, the first amino acid of the processed HFE chain as identified by N-terminal sequencing is residue 1; previous numbering systems starting at the initial methionine of the signal peptide refer to it as 23 (Cuthbert, 1997, and references therein).

Purified HFE or the control proteins FcRn and UL18 (0.25 mg of each) were treated with acetic acid and analyzed for the presence of bound peptides using established methods (Rötzschke et al., 1990) as previously described for UL18 and FcRn (Chapman and Bjorkman, 1998). Low–molecular weight filtrates of the acid eluates were lyophilized, and half of each eluate was analyzed by automated Edman degradation using an Applied Biosystems model 477A protein sequencer for pool sequencing (Table 2).

Crystallization and Data Collection

Crystals (space group $P2_12_12_1$; a = 68.8 Å, b = 100.1 Å, c = 147.6 Å; two molecules per asymmetric unit) of HFE were grown in 1:1 hanging drops containing Vibrio cholerae neuraminidase–treated HFE (14 mg/ml) and 16% (w/v) PEG 4000, 0.4 M ammonium acetate, and 0.1 M sodium citrate (pH 5.9), then improved by microseeding and macroseeding. Before data collection, crystals were transferred to a cryoprotectant solution (22% PEG 4000, 0.4 M ammonium acetate, 0.1 M sodium citrate [pH 5.9] and 7.5% glycerol). Initial data were collected at −150°C from a single crystal to 2.9 Å using a MAR Research detector at the Stanford Synchrotron Radiation Laboratory beamline 7–1. A second dataset was collected to 2.6 Å using Fuji image plates and an off-line scanner at the Brookhaven National Laboratory beamline X4A. The diffraction was anisotropic, extending beyond 2.0 Å along c* and to 2.6 Å along a* and b*. Data were processed and scaled with DENZO and SCALEPACK (Otwinowski and Minor, 1996) (Table 1).

Structure Determination and Refinement

The structure was determined by molecular replacement using AMoRe (Navaza, 1994). A self-rotation function (15.0–4.0 Å) revealed a noncrystallographic 2-fold axis positioned at 45° in the x-y plane. Cross-rotation and -translation functions (15.0–4.0 Å) using the 2.0 Å structure of HLA-A2 (PDB code 2CLR with the peptide omitted, nonconserved side chains truncated to alanine, residues 124–156 deleted) as a search model yielded a solution for the first molecule (correlation coefficient: 26.6%; R factor of 55.0%). The second molecule was found in a partial translation function with the first molecule fixed in which the coordinates for the first molecule were rotated according to the noncrystallographic 2-fold and used as a search model (correlation coefficient: 29.7%; R factor of 53.2%). Rigid body refinement (6.0–3.5 Å) of both molecules resulted in an R_{cryst} of 50.9% (R_{free} = 50.5%). Averaged and solvent-flattened maps calculated to 2.9 Å with DM (Cowtan, 1994) showed density for residues 124–156 and the α1 helix (shifted ~4 Å relative to HLA-A2). Residues 124–156 were modeled using O (Jones and Kjeldgaard, 1997), and the α1 helix was positioned by rigid body refinement. Further rebuilding was done using averaged simulated annealing $F_o\Phi_{ave}$ omit maps (Hodel et al., 1992) (throughout the model in ~10% increments) and conventional $(2F_o-F_c)\Phi_{calc}$ and $(F_o-F_c)\Phi_{calc}$ maps. Anisotropy and bulk solvent corrections were applied, and the model was refined against the Brookhaven dataset (15–2.6 Å) with tight NCS restraints (300 kcal/mol·Å^2) and individual temperature (B) factors using XPLOR (Brünger, 1992a). Despite the relatively high mean B factor

each representing the indicated percent of the total binding sites.

(A) Plots of equilibrium binding response (R_{eq}) versus the log of the concentration of injected protein derived from biosensor experiments in which the binding response closely approached or reached equilibrium. Best-fit binding curves to the experimental data points are shown as continuous lines. K_D's derived from independent experiments performed on chips coupled to different densities agreed to within a factor of two.

(B) Sensorgrams (thick colored lines) from kinetics-based experiments overlaid with the calculated response (thin black lines) derived using the model indicated on each panel. One representative set of injections from experiments performed in triplicate is shown for each interaction (analyses from triplicate experiments reported in Table 4).

(C) Sensorgrams from kinetics-based experiments using TfR noncovalently coupled to a Ni-NTA chip. The HFE→TfR analysis is complicated by a significant interaction of HFE with the Ni-NTA chip itself (blank responses and their corresponding binding responses after blank subtraction are shown in the same color). Because the blanks represent a high proportion (more than half) of the total binding, the resulting subtracted curves do not yield a precise value for the K_D.

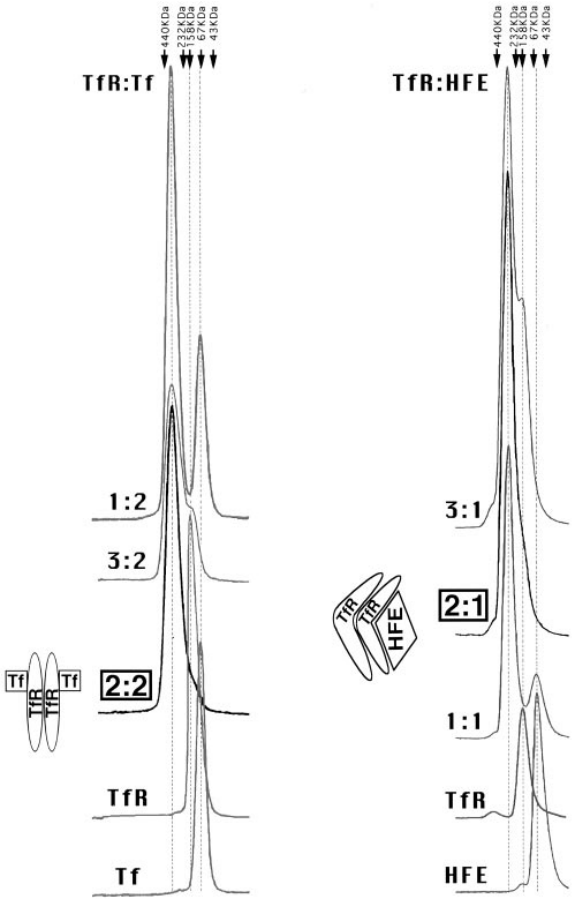

Figure 4. Gel Filtration Chromatographic Demonstration that TfR Binds to Tf and to HFE with Different Stoichiometries

TfR and Fe-Tf (left panel) or TfR and HFE (right panel) were incubated at pH 7.4 at the indicated molar ratios, then passed over a sizing column to separate TfR:Tf or TfR:HFE complexes from uncomplexed proteins. At a 2:2 molar ratio of TfR to Tf and a 2:1 molar ratio of TfR to HFE, virtually all of the protein chromatographed as the complex. When the input ratio of TfR to Tf was greater than 2:2 there was excess TfR, and when it was less than 2:2 there was excess Tf (verified by SDS-PAGE analysis; data not shown). Likewise, when the input ratio of TfR to HFE was greater than 2:1 there was excess TfR, and when it was less than 2:1 there was excess HFE. Schematic representations of the TfR:Tf and TfR:HFE complexes shown beside the chromatograms are consistent with the data, but do not represent the only possible models accounting for the different stoichiometries.

of 62 Å^2 (Wilson B factor = 67 Å^2), the model is generally well defined in the electron density (Figure 1C). The model (R_{cryst} = 23.3%; R_{free} = 27.7%) includes 272 out of 275 residues in the recombinant HFE heavy chain and all 99 of the residues in β2m. No ordered density was observed for carbohydrate at the three potential N-linked glycosylation sites at positions 88, 108, and 212. A large difference electron density peak near Phe-76 in an apolar pocket was not conclusively identified but was modeled as water in the absence of other chemical information. Residues 1–3 are not seen in the electron density and 14 side chains are disordered and were modeled as alanines (HFE residues 18, 42, 53–57, 63, 66–67, 106, and 177; β2m residues 48 and 75). Several regions in loops include residues with real space correlation values (Jones and Kjeldgaard, 1997) below one standard deviation from the mean (residues 17–23, 53–61, 90–91, 106–108, 174–176, 225–230).

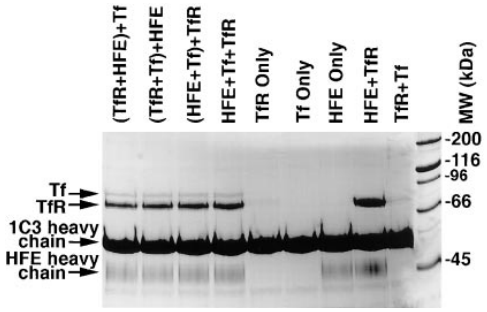

Figure 5. TfR, Tf, and HFE Can Form a Ternary Complex

Individual proteins or mixtures of proteins were immunoprecipitated with 1C3 (anti-HFE) and analyzed on a 10% reducing SDS-PAGE gel (conditions chosen to maximize separation between TfR and Tf). Proteins listed in parentheses were incubated together first, followed by addition of the third protein. The β2m light chain of HFE and the antibody light chain are present on gels composed of a higher percentage of acrylamide (data not shown).

Comparisons to Class I-Related Proteins and Analyses of Groove Surfaces

Alignments were performed with LSQMAN (Kleywegt, 1996) (3.0 Å maximum matching distance for Cα pairs). Rms deviations for HFE superimposed with HLA-A2 (PDB code 2CLR): 1.5 Å (α1; 71 Cα's), 1.2 Å (α2; 83 Cα's), and 0.8 Å (α3; 76 Cα's); FcRn (PDB code 1FRU) superimposed with HLA-A2: 1.1 Å (α1; 62 Cα's), 1.6 Å (α2; 75 Cα's), and 1.3 Å (α3; 77 Cα's); CD1 superimposed with HLA-A2: 1.2 Å (α1; 47 Cα's), 1.5 Å (α2; 71 Cα's), and 1.3 Å (α3; 81 Cα's).

Groove surface areas were calculated as follows. First, groove residues were identified as those having ≥5.0 Å^2 of solvent-accessible surface area using a 1.4 Å probe radius but <5.0 Å^2 of solvent-accessible surface area calculated using a 5.0 Å probe radius in XPLOR (Brünger, 1992a). Using GRASP (Nicholls et al., 1991), we then (i) built a molecular surface of only the groove residues, (ii) selected the contiguous groove surface between the α1 and α2 helices by scribing its perimeter, and (iii) calculated its surface area. This residue-based method of calculating groove surface areas differs from the atom-based method described by Zeng et al. (1997). For comparison, we also used the atom-based method, which yielded estimates for the groove surface areas in HFE (~410 Å^2), class I (~690 Å^2), and CD1 (~1390 Å^2) that were similar both to the values calculated with the residue-based method (see text) and to values previously reported (Zeng et al., 1997). However, we were unable to define a contiguous groove surface for FcRn using the atom-based method. The residue-based method yields a value of ~235 Å^2, approximately half of the value reported by Zeng et al. (1997), presumably because the grooves were defined differently.

Expression, Purification, and Characterization of TfR

A soluble version of TfR, normally a type II membrane glycoprotein (Schneider et al., 1984), was expressed in a lytic baculovirus/insect cell expression system. The portion of the human TfR gene encoding residues 121–760 (the C-terminal amino acid of wild-type TfR) was fused 3′ to a gene segment encoding the hydrophobic leader peptide from the baculovirus protein gp67, a 6xHis-tag, and a factor X_a cleavage site in a modified version of the pAcGP67A expression vector (Pharmingen). The N-terminal start site for soluble TfR was chosen based on studies of a previously characterized soluble proteolytic fragment of TfR beginning at residue 121, which has been crystallized (Borhani and Harrison, 1991) and forms a stable dimer that binds Tf, although it lacks two interchain disulfides involving Cys-89 and Cys-98 (Turkewitz et al., 1988a). Recombinant virus was generated by cotransfection of the transfer vector with linearized viral DNA (Baculogold; Pharmingen). TfR was purified from supernatants of baculovirus-infected High 5 cells using Ni-NTA chromatography (Ni-NTA superflow; Qiagen) followed by gel filtration chromatography using a Superdex-200 FPLC column (Pharmacia). A far UV

Table 4. Biosensor Analyses of TfR Binding to Tf and HFE

	$K_{D,eq}$[a] (nM)	$K_{D,calc}$[b](nM)	k_a (sec^{-1} M^{-1})	k_d (sec^{-1})
TfR immobilized				
Fe-Tf (pH 7.5)[c]	*	5.7	3.1×10^5	1.8×10^{-3}
Fe-Tf (pH 7.5)[d]	1.9	0.81 ± 0.1	$(1.6 \pm 0.04) \times 10^6$	$(1.3 \pm 0.2) \times 10^{-3}$
apo-Tf (pH 6.0)[e]	<15	1.3 ± 0.2	$(7.3 \pm 0.7) \times 10^5$	$(9.4 \pm 2) \times 10^{-4}$
apo-Tf + PP_i (pH 7.5)[e]	>8,000	N.B.	N.B.	N.B.
HFE (pH 7.5)[f]	350	130 ± 10	$(8.1 \pm 0.9) \times 10^5$	$(1.1 \pm 0.1) \times 10^{-1}$
HFE (pH 6.0)[f]	>10,000	N.B.	N.B.	N.B.
HFE immobilized				
TfR (pH 7.5)[g]	0.91	0.33 ± 0.02	$(3.8 \pm 0.2) \times 10^6$	$(1.2 \pm 0.1) \times 10^{-3}$
TfR (pH 6.0)[g]	*	N.B.	N.B.	N.B.
Fe-Tf (pH 7.5)[g]	N.B.	N.B.	N.B.	N.B.
apo-Tf (pH 6.0)[g]	N.B.	N.B.	N.B.	N.B.

* Not determined because the experiment could not be performed (see Experimental Procedures).
N.B. No significant binding at concentrations up to 1 μM.
[a] Determined from equilibrium binding data. Only the higher affinity of two noninteracting binding sites is reported when binding curves were fit to a model assuming two independent classes of binding sites (see Figure 3A).
[b] Determined from the ratio of the kinetic constants (k_d/k_a) from experiments performed in triplicate when a standard deviation is given. Only the higher affinity of two noninteracting binding sites is reported when sensorgrams were fit to a model assuming two independent classes of binding sites (see Figure 3B).
[c] 6xHis-tagged TfR was noncovalently immobilized to a density of 220 RU on an Ni-NTA sensor chip (Figure 3C).
[d] TfR was covalently immobilized to a density of 2310 RU for the equilibrium experiments and 420 RU for the kinetic experiments.
[e] TfR was covalently immobilized to a density of 1460 RU for the equilibrium experiments and 420 RU for the kinetic experiments. The equilibrium measurements at pH 6 did not fully equilibrate during the injection time, thus 15 nM is the upper limit for the K_D. 10 mM PP_i was added to the buffer at pH 7.5 to prevent loading of apo-Tf with trace amounts of iron in the buffers.
[f] TfR was covalently immobilized to a density of 1600 RU for the equilibrium experiments and 420 RU for the kinetic experiments.
[g] HFE was covalently immobilized to a density of 3800 RU for the equilibrium experiments and 418 RU for the kinetic experiments.

CD spectrum of the purified protein (data not shown) verified folding and resembled the spectrum of the proteolytic fragment of TfR (Turkewitz et al., 1988b).

Biosensor-Based Affinity Measurements

A BIAcore 1000 biosensor system (Pharmacia LKB Biotechnology) was used to assay interactions between HFE, TfR, and human Tf (Sigma; Fe-Tf was further purified by gel filtration chromatography). Binding between a molecule coupled to a biosensor chip and a second molecule injected over the chip results in changes in the SPR signal that are read out in real time as resonance units (RU) (Malmqvist and Granzow, 1994). We derived equilibrium dissociation constants (K_D's) whenever possible using two methods. In the first ($K_{D,eq}$ column in Table 4), binding reactions were allowed to closely approach or to reach equilibrium by using long injections (50 min) with slow flow rates (5 μl/min) over biosensor chips coupled to high densities (>1000 RU). $K_{D,eq}$ values were derived by nonlinear regression analysis of plots of R_{eq} (the equilibrium binding response) versus the log of the concentration of the injected protein (Figure 3A). The fit of data to binding models assuming one or more classes of interacting or noninteracting binding sites was then examined, and the appropriate model was chosen as described (Vaughn and Bjorkman, 1997). In the second method ($K_{D,calc}$ in Table 4; $K_{D,calc} = k_d/k_a$; k_a and k_d are the association and dissociation rate constants, respectively), kinetic constants were derived from binding experiments conducted for shorter times (2–4 min) using faster flow rates (50 μl/min) over chips coupled at lower densities (~400 RU). These conditions were chosen to minimize mass transport effects upon the kinetics of binding reactions (Karlsson and Fält, 1997), which are not a concern for the equilibrium measurements. Kinetic constants were derived from sensorgram data using simultaneous fitting to the association and dissociation phases of the interaction and global fitting to all curves in the working set (Figures 3B and 3C) as implemented in BIAevaluation version 3.0.

TfR (20 μg/ml in 5 mM maleate [pH 6.0]) or HFE (55 μg/ml in 20 mM sodium acetate [pH 5.0]) was immobilized using standard amine coupling chemistry on a CM5 chip (Pharmacia LKB Biotechnology). Higher coupling densities for the equilibrium-based experiments were achieved by increasing the time of exposure of the protein solutions to the activated flowcell. For the kinetic experiments involving TfR, the 6xHis-tag was removed by factor X_a (New England Biolabs) treatment according to the manufacturer's instructions, followed by purification on a Biospin column (Biorad). Proteins were injected at room temperature in 50 mM PIPES (pH 6.0 or pH 7.5), 150 mM NaCl, 0.005% BIAcore surfactant P20. All injections onto a TfR- or HFE-coupled flowcell were followed by an identical injection onto a mock-coupled flowcell or a flowcell coupled with an irrelevant protein in order to subtract out significant nonspecific responses.

To achieve a defined orientation and to avoid exposing TfR to the low pH conditions required for primary amine coupling (which produce a conformational change resulting in self-association at pH <6 [Turkewitz et al., 1988b]; J. A. L., P. J. B., and P. Poon, unpublished data), we injected soluble HFE over 6xHis-tagged TfR noncovalently coupled to a biosensor chip derivatized with Ni-NTA. Only kinetic experiments were performed using this chip, since the amount of His-tagged TfR released from the Ni-NTA chip became significant during the long injections required for the equilibrium-based measurements. The Ni-NTA chip could not be used for binding studies at pH 6.0, as the 6xHis interaction with nickel is not stable at this pH.

Gel Filtration Analyses of TfR-Tf and TfR-HFE Stoichiometries

Protein concentrations were determined spectrophotometrically at 280 nm using the following extinction coefficients: HFE, 96570 $M^{-1}cm^{-1}$; TfR monomer, 93790 $M^{-1}cm^{-1}$; Tf, 83360 $M^{-1}cm^{-1}$. Extinction coefficients were first calculated from the protein sequences, then A_{280} measurements for a fixed amount of each protein were compared in 6 M GuHCl and aqueous solutions and the coefficient was adjusted if necessary. For the TfR:Tf experiments, molar ratios from 3:2 to 1:2 of TfR and Fe-Tf were incubated for 20 min at room temperature in 20 mM Tris (pH 7.4), 150 mM NaCl, 0.02% NaN_3, keeping the amount of TfR fixed at 200 pmol in a total volume of 25 μl. For the TfR:HFE experiments, molar ratios from 3:1 to 1:1 of TfR and HFE were incubated as described above, keeping the amount of HFE fixed at 360 pmol in a total volume of 25 μl. Samples (25 μl) were injected onto a Superose 6B FPLC column (Pharmacia), eluted with the same buffer at 0.5 ml/min, and the fractions analyzed by SDS-PAGE (data not shown).

Coimmunoprecipitation of HFE, TfR, and Tf in a Ternary Complex

TfR (138 pmol), Fe-Tf (138 pmol), and HFE (69 pmol) were incubated for 15 min at room temperature in 20 mM Tris (pH 7.4), 150 mM NaCl, 0.025% NaN_3 (incubation buffer). All three proteins were incubated for 15 min or two of the proteins were preincubated for 15 min, followed by addition of the third protein and a second 15 min incubation. The reaction mixture was then diluted from 130 μl to 1 ml using the same buffer, and 5 μl of ascites containing the 1C3 anti-HFE monoclonal antibody were added. After incubation for 60 min at room temperature, 30 μl of protein G beads (Pharmacia; 2 mg of protein G/ml of beads) were added, and incubated with mixing for 60 min. After pelleting, the beads were washed once with incubation buffer, twice with phosphate buffered saline, 0.05% Tween 20 (Sigma), and once again with incubation buffer, then boiled in 20 μl of SDS-PAGE loading buffer containing 10% (v/v) 2-mercaptoethanol and loaded onto a 10% SDS-PAGE gel (Figure 5). Bands corresponding to the individual proteins were identified by comparison with the migration of samples of purified proteins (data not shown).

Acknowledgments

We thank T. L. Chapman for performing the acid elutions, I. Nangiana and D. Penny for assistance with protein expression, the Caltech PPMAL for peptide and protein analyses, Drs. C. Ogata and M. Soltis for assistance with synchrotron data collection, Drs. I. A. Wilson and B. Segelke for providing CD1 coordinates prior to PDB release and helpful discussions regarding groove surface area calculations, Dr. P. Poon for performing the analytical ultracentrifugation studies of TfR, and Dr. L. Sánchez for critical reading of the manuscript. M. J. B. was supported by a grant from the Cancer Research Institute, and J. A. L. was supported by a FORD fellowship. Atomic coordinates for HFE have been deposited with the Protein Data Bank.

Received January 16, 1998; revised February 26, 1998.

References

Bacon, B.R., and Tavill, A.S. (1996). Hepatology: A Textbook of Liver Disease. (Philadelphia: Saunders).

Bebbington, C.R., and Hentschel, C.C.G. (1987). DNA Cloning. (Oxford: IRL).

Beckman, E.M., Porcelli, S.A., Morita, C.T., Behar, S.M., Furlong, S.T., and Brenner, M.B. (1994). Recognition of a lipid antigen by CD1-restricted (αβ+) T cells. Nature *372*, 691–694.

Beutler, E. (1997). The significance of the 187G (H63D) mutation in hemochromatosis. Am. J. Hum. Genet. *61*, 762–764.

Borhani, D.W., and Harrison, S.C. (1991). Crystallization and X-ray diffraction studies of a soluble form of the human transferrin receptor. J. Mol. Biol. *218*, 685–689.

Brünger, A.T. (1992a). XPLOR Version 3.1 A System for X-ray Crystallography and NMR. (New Haven: Yale University Press).

Brünger, A.T. (1992b). Free R value: a novel statistical quantity for assessing the accuracy of crystal structures. Nature *355*, 472–475.

Burmeister, W.P., Gastinel, L.N., Simister, N.E., Blum, M.L., and Bjorkman, P.J. (1994a). Crystal structure at 2.2 Å resolution of the MHC-related neonatal Fc receptor. Nature *372*, 336–343.

Burmeister, W.P., Huber, A.H., and Bjorkman, P.J. (1994b). Crystal structure of the complex of rat neonatal Fc receptor with Fc. Nature *372*, 379–383.

Castaño, A.R., Tangri, S., Miller, J.E.W., Holcombe, H.R., Jackson, M.R., Huse, W.D., Kronenberg, M., and Peterson, P.A. (1995). Peptide binding and presentation by mouse CD1. Science *269*, 223–226.

Chapman, T.L., and Bjorkman, P.J. (1998). Characterization of a murine cytomegalovirus class I major histocompatibility complex (MHC) homolog: comparison to MHC molecules and to the human cytomegalovirus MHC homolog. J. Virol. *72*, 460–466.

Collins, E.J., Garboczi, D.N., and Wiley, D.C. (1994). Three-dimensional structure of a peptide extending from one end of a class I MHC binding site. Nature *371*, 626–629.

Cowtan, K. (1994). Joint CCP4 and ESF-EACBM Newsletter on Protein Crystallography *31*, 34–38.

Cuthbert, J.A. (1997). Iron, *HFE*, and hemochromatosis update. J. Invest. Med. *45*, 518–529.

Enns, C.A., and Sussman, H.H. (1981). Physical characterization of the transferrin receptor in human placentae. J. Biol. Chem. *256*, 9820–9823.

Feder, J.N., Gnirke, A., Thomas, W., Tsuchihashi, Z., Ruddy, D.A., Basava, A., Dormishian, F., Domingo, R., Ellis, M.C., Fullan, A., et al. (1996). A novel MHC class I-like gene is mutated in patients with hereditary hemochromatosis. Nature Genet. *13*, 399–408.

Feder, J.N., Tsuchihashi, Z., Irrinki, A., Lee, V.K., Mapa, F.A., Morikang, E., Prass, C.E., Starnes, S.M., Wolff, R.K., Parkkila, S., et al. (1997). The hemochromatosis founder mutation in HLA-H disrupts β2-microglobulin interaction and cell surface expression. J. Biol. Chem. *272*, 14025–14028.

Feder, J.N., Penny, D.M., Irrinke, A., Lee, V.K., Lebrón, J.A., Watson, N., Tsuchihashi, Z., Sigal, E., Bjorkman, P.J., and Schatzman, R.C. (1998). The hemochromatosis gene product complexes with the transferrin receptor and lowers its affinity for ligand binding. Proc. Natl. Acad. Sci. USA *95*, 1472–1477.

Fersht, A. (1985). Enzyme Structure and Mechanism, 2nd Edition. (New York: W.H. Freeman and Company).

Hashimoto, K., Hirai, M., and Kurosawa, Y. (1997). Identification of a mouse homolog for the human hereditary haemochromatosis candidate gene. Biochem. Biophys. Res. Comm. *230*, 35–39.

Hodel, A., Kim, S.-H., and Brunger, A.T. (1992). Model bias in macromolecular structures. Acta Crystallogr. A *48*, 851–858.

Howard, J.B., and Rees, D.C. (1991). Perspectives on non-heme iron protein chemistry. Adv. Protein Chem. *42*, 199–280.

Jones, T.A., and Kjeldgaard, M. (1997). Electron density map interpretation. Meth. Enzymol. *277*, 173–208.

Junghans, R.P. (1997). Finally! The Brambell receptor (FcRB). Mediator of transmission of immunity and protection from catabolism for IgG. Immunol. Res. *16*, 29–57.

Karlsson, R., and Fält, A. (1997). Experimental design for kinetic analysis of protein–protein interactions with surface plasmon resonance biosensors. J. Immunol. Methods *200*, 121–133.

Kleywegt, G.J. (1996). Use of non-crystallographic symmetry in protein structure refinement. Acta Crystallogr. D *52*, 842–857.

Kleywegt, G.J., and Jones, T.A. (1996). Phi/Psi-chology: Ramachandran revisited. Structure *4*, 1395–1400.

Kraulis, P. (1991). MOLSCRIPT: a program to produce both detailed and schematic plots of protein structures. J. Appl. Crystallogr. *24*, 946–950.

Kuziemko, G.M., Stroh, M., and Stevens, R.C. (1996). Cholera toxin binding affinity and specificity for gangliosides determined by surface plasmon resonance. Biochemistry *35*, 6375–6384.

Madden, D.R., Garboczi, D.N., and Wiley, D.C. (1993). The antigenic identity of peptide-MHC complexes: a comparison of five viral peptides presented by HLA-A2. Cell *75*, 693–708.

Malmqvist, M., and Granzow, R. (1994). Biomolecular interaction analysis. Methods *6*, 95–98.

Matsumura, M., Fremont, D.H., Peterson, P.A., and Wilson, I.A. (1992). Emerging principles for the recognition of peptide antigens by MHC class I molecules. Science *257*, 927–934.

McLaren, G.D., Nathanson, M.H., Jacobs, A., Trevett, D., and Thomson, W. (1991). Regulation of intestinal iron absorption and mucosal iron kinetics in hereditary hemochromatosis. J. Lab. Clin. Med. *117*, 390–410.

Merritt, E.A., and Murphy, M.E.P. (1994). Raster3D Version 2.0—a program for photorealistic molecular graphics. Acta Crystallogr. D *50*, 869–873.

Merryweather-Clarke, A.T., Pointon, J.J., Shearman, J.D., and Robson, K.J. (1997). Global prevalence of putative haemochromatosis mutations. J. Med. Genet. *34*, 275–278.

Navaza, J. (1994). AMoRe: an automated package for molecular replacement. Acta Crystallogr. A *50*, 157–163.

Nicholls, A., Sharp, K.A., and Honig, B.H. (1991). Protein folding

and association: insights from the interfacial and thermodynamic properties of hydrocarbons. Proteins *11*, 281–296.

Otwinowski, Z., and Minor, W. (1996). Processing of X-ray diffraction data collected in oscillation mode. Meth. Enzymol. *276*, 307–326.

Parkkila, S., Waheed, A., Britton, R.S., Bacon, B.R., Zhou, X.Y., Tomatsu, S., Fleming, R.E., and Sly, W.S. (1997). Association of the transferrin receptor in human placenta with HFE, the protein defective in hereditary hemochromatosis. Proc. Natl. Acad. Sci. USA *94*, 13198–13202.

Rammensee, H.-G., Falk, K., and Rötzschke, O. (1993). Peptides naturally presented by MHC class I molecules. Annu. Rev. Immunol. *11*, 213–244.

Richardson, D.R., and Ponka, P. (1997). The molecular mechanisms of the metabolism and transport of iron in normal and neoplastic cells. Biochim. Biophys. Acta *1331*, 1–40.

Rötzschke, O., Falk, K., Deres, K., Schild, H., Norda, M., Metzger, J., Jung, G., and Rammensee, H.-G. (1990). Isolation and analysis of naturally processed viral peptides as recognized by cytotoxic T cells. Nature *348*, 252–257.

Saper, M.A., Bjorkman, P.J., and Wiley, D.C. (1991). Refined structure of the human histocompatibility antigen HLA-A2 at 2.6 Å resolution. J. Mol. Biol. *219*, 277–319.

Schneider, C., Owen, M.J., Banville, D., and Williams, J.G. (1984). Primary structure of human transferrin receptor deduced from the mRNA sequence. Nature *311*, 675–678.

Turkewitz, A.P., Amatruda, J.F., Borhani, D., Harrison, S.C., and Schwartz, A.L. (1988a). A high yield purification of the human transferrin receptor and properties of its major extracellular fragment. J. Biol. Chem. *263*, 8318–8325.

Turkewitz, A.P., Schwartz, A.L., and Harrison, S.C. (1988b). A pH-dependent reversible conformational transition of the human transferrin receptor leads to self-association. J. Biol. Chem. *263*, 16309–16315.

Vaughn, D.E., and Bjorkman, P.J. (1997). High affinity binding of the neonatal Fc receptor to its IgG ligand requires receptor immobilization. Biochemistry *36*, 9374–9380.

Vaughn, D.E., and Bjorkman, P.J. (1998). Structural basis of pH dependent antibody binding by the neonatal Fc receptor. Structure *6*, 63–73.

Waheed, A., Parkkila, S., Zhou, X.Y., Tomatsu, S., Tsuchihashi, Z., Feder, J.N., Schatzman, R.C., Britton, R.S., Bacon, B.R., and Sly, W.S. (1997). Hereditary hemochromatosis: effects of C282Y and H63D mutations on association with β2-microglobulin, intracellular processing, and cell surface expression of the HFE protein in COS-7 cells. Proc. Natl. Acad. Sci. USA *94*, 12384–12389.

Zeng, Z.-H., Castaño, A.R., Segelke, B.W., Stura, E.A., Peterson, P.A., and Wilson, I.A. (1997). Crystal structure of mouse CD1: an MHC-like fold with a large hydrophobic binding groove. Science *277*, 339–345.